PAUL SCHERRER INSTITUT

PSI-PR-99-08
February 1999

Kinetic Energy Distribution of $\pi^- p$ - atoms in Liquid and Gaseous Hydrogen

A. Badertscher[2], M. Daum[1,a], P.F.A. Goudsmit[2], M. Janousch[2,b], P.-R. Kettle[1], J. Koglin[1,3], V.E. Markushin[1], J. Schottmüller[1,4], Z.G. Zhao[2,c]

[1] PSI, Paul Scherrer Institut, CH-5232 Villigen PSI, Switzerland.
[2] IPP, Institute for Particle Physics, ETH Zürich, CH-8093 Zürich, Switzerland.
[3] Physics Department, University of Virginia, Charlottesville, Virginia 22901, USA.
[4] Physik-Institut der Universität Zürich, Winterthurer Strasse 190, CH-8057 Zürich, Switzerland.

[a] E-mail address: Manfred.Daum@psi.ch
Tel.: ++41 56 310 36 68; Fax: ++41 56 310 32 94
[b] Present address: PSI, Paul Scherrer Institut, CH-5232 Villigen PSI, Switzerland.
[c] Present address: Institute of High Energy Physics, Chinese Academy of Science, Beijiing 100039, The People's Republic of China

Paul Scherrer Institut
CH - 5232 Villigen PSI
Telefon 056 310 21 11
Telefax 056 310 21 99

Kinetic energy distribution of $\pi^- p$-atoms in liquid and gaseous hydrogen

A. Badertscher[2], M. Daum[1,a], P. F. A. Goudsmit[2], M. Janousch[2,b], P.-R. Kettle[1], J. Koglin[1,3], V. E. Markushin[1], J. Schottmüller[1,4], Z. G. Zhao[2,c]

[1]PSI, Paul-Scherrer-Institut, CH-5232 Villigen-PSI, Switzerland.
[2]IPP, Institute for Particle Physics, ETH Zürich, CH-8093 Zürich, Switzerland.
[3]Physics Department, University of Virginia, Charlottesville, Virginia 22901, USA.
[4]Physik-Institut der Universität Zürich, Winterthurer Str. 190, CH-8057 Zürich, Switzerland

[a]E-mail address: Manfred.Daum@PSI.CH;
Tel.: +41 56 310 36 68; Fax: +41 56 310 32 94.
[b]Present address:
PSI, Paul-Scherrer-Institut, CH-5232 Villigen-PSI, Switzerland.
[c]Present address:
Institute of High Energy Physics, Chinese Academy of Science, Beijing 100039, The People's Republic of China.

ABSTRACT

We have measured the Doppler broadening of neutron time-of-flight spectra from the reaction $\pi^- p \to \pi^0 + n$ in atomic states. From the data, we infer that the kinetic energy distribution of $\pi^- p$-atoms in liquid and gaseous hydrogen contains discrete 'high-energy' components with energies as high as 200 eV attributed to Coulomb de-excitation. In liquid hydrogen, evidence for Coulomb de-excitation transitions with $\Delta n = 2$ has been found.

PACS: 36.10.Gv; 25.80.Fm; 13.75.Gx

In previous experiments, in which the pion mass difference $m_{\pi^-} - m_{\pi^0}$ was determined from the time-of-flight (TOF) of neutrons emitted in the charge-exchange (CEX) reaction $\pi^- p \to \pi^0 + n$ in liquid hydrogen, a substantial fraction of highly energetic ($\gg 1\,\mathrm{eV}$) $\pi^- p$-atoms was reported [1–4]. The effect, observed as a Doppler broadening of the neutron time-of-flight (TOF) peak, is related to the kinetic energy distribution $f(T_{\pi p})$ of $\pi^- p$-atoms at the instant of the CEX-reaction. However, the originally reported value of the broadening by Czirr [1] gives a value for the mean kinetic energy of the $\pi^- p$-atoms in disagreement with that found by Crawford et al. [4]. Later experiments gave further evidence for such 'high-energy' components in liquid hydrogen in agreement with pu Ref. [4] and in hydrogen gas [5, 6]. A precise knowledge of the kinetic energy distribution of the pionic hydrogen atoms is important in the determination of the strong interaction width of the $\pi^- p$ ground state from the measurement of pionic X-ray transitions [7–10].

The observed Doppler broadening of the TOF-spectra [1–6] can be attributed to Coulomb de-excitation [11] $(\pi^- p)_n + p \to (\pi^- p)_{n'} + p$ [1], where the de-excitation energy associated with the transition is shared as kinetic energy between the collision partners. Other cascade processes, such as external Auger effect, are only able to cause a moderate acceleration of the pionic atom ($\sim 1\,\mathrm{eV}$) [14].

The kinetic energy of the $\pi^- p$-atom after a Coulomb de-excitation transition is given by

$$T_{nn'} = \Delta E_{nn'}/(1 + M_{\pi p}/m_p), \tag{1}$$

neglecting the initial kinetic energy of the pionic atom. Here, $\Delta E_{nn'}$ is the energy difference of the two atomic states with principal quantum numbers n and n'; $M_{\pi p}$ and m_p are the masses of the $\pi^- p$-atom and the proton, respectively. The corresponding idealized energy distribution $f(T_{\pi p})$ is shown in Fig. 1(a), where only transitions with $\Delta n = 1$ are considered. For the sake of simplicity, the low energy part of $f(T_{\pi p})$ is approximated by a uniform distribution between 0 and T_1. This $T_{\pi p}$-distribution [Fig. 1(a)] leads to the step-like neutron TOF-distribution shown in Fig. 1(b), where τ is the difference between TOF (t) and the mean TOF (t_0). The times τ_1 and $\tau_{nn'}$ in Fig. 1(b) are related to the kinetic energies T_1 and $T_{nn'}$ as

[1] It is not excluded that Coulomb de-excitation is part of some new mechanism, e.g. the formation of a resonant state, as was discussed for $n = 2$ [12, 13].

follows [15]:

$$\tau_1 = \frac{l}{v_0^2}\sqrt{\frac{2T_1}{M_{\pi p}}}, \qquad \tau_{nn'} = \frac{l}{v_0^2}\sqrt{\frac{2T_{nn'}}{M_{\pi p}}}. \tag{2}$$

Here, l is the length of the flight-path, and $v_0 = 0.894\,\mathrm{cm/ns}$ is the neutron velocity for $\pi^- p$-atoms undergoing the CEX-reaction at rest. At this point, we assume that the $\pi^- p$-atoms are not significantly decelerated between Coulomb de-excitation and nuclear capture. This assumption is supported by cascade calculations [6] for atoms with a kinetic energy of $T \geq 50\,\mathrm{eV}$. Therefore, a signature for Coulomb de-excitation would be a step-like structure visible in the TOF-spectra of neutrons from the CEX-reaction. For atoms with $T \leq 20\,\mathrm{eV}$, the deceleration is important, and the Coulomb peaks are expected to be smeared out.

The present experiment was performed at the πE1-channel of PSI; the experimental setup is shown in Fig. 2. The following improvements to the previous experiment [5] were made: (i) a reduction of the background by introducing several neutron collimators as well as using specially selected low noise photomultiplier (PM) tubes for the neutron counters; (ii) improvement of the time resolution of the neutron counters by placing them in adjustable holders so as to point radially at the target for the different neutron flight-paths; (iii) increased counting statistics by enlarging the solid angle of the neutron detector and using a new beamline setup.

Pions of 117 MeV/c passed the beam counter S1 (see Fig. 2) and a carbon degrader, the thickness of which was optimized for a maximal stop rate in the hydrogen target. The liquid target (LH_2) had a length of 9.3 cm in the direction of the pion beam and a thickness of 0.5 cm in the direction of the neutron flight-path perpendicular to the pion beam. The 40 bar gas target was operated at room temperature and had a length of 21.2 cm in the direction of the pion beam and a diameter of 14 mm. Neutrons from the hydrogen target were detected after a flight-path of variable length (3 – 11 m) in a detector array consisting of 36 scintillator disks coupled directly to PM-tubes. For the measurements in liquid hydrogen, we used PILOT-U scintillators with a thickness of 5 mm, whereas for the measurements in gas, NE102A scintillators with a thickness of 15 mm were used in order to partially compensate for the lower pion stop density. The neutrons from the CEX-reaction in the target were accepted only if coincident with a suitably delayed π-stop signal and a corresponding γ-ray signal from π^0-decay in a NaI-calorimeter [16].

The data are in form of TOF (TDC) and pulse-height (ADC) distributions. In

a first step of the analysis, which is very similar to that of Ref. [5], a lower and an upper ADC-cut were introduced for each neutron counter separately, in order to suppress noise events from the PMs (lower ADC-cut) and accidental events triggered by photons from the π^0-decays, radiative capture and bremsstrahlung from beam electrons (upper ADC-cut). Both ADC-cuts were optimized for a maximal signal-to-noise ratio for each neutron counter separately. Before summing the spectra of all 36 neutron counters, the centre of each neutron peak was shifted by a few TDC-channels to the same channel number in order to correct for small transit time differences in the PMs and cables as well as small differences in the individual neutron flight-paths.

In a second step, cuts were applied to the summed photon energy from the NaI-calorimeter, accepting only events between 60 and 110 MeV. In this way, photons from bremsstrahlung and from the $\pi^- p \rightarrow \gamma n$ reaction were suppressed. These cuts were also optimized for a maximal signal-to-noise ratio. The small remaining background in the TOF-spectra, consisting of a flat component from noise events and accidental peaks from π^0-decays, bremsstrahlung and 130 MeV photons from the reaction $\pi^- p \rightarrow \gamma n$, was determined and subtracted as discussed previously [4].

The resulting TOF-spectra, taken at 3.82 m, 8.39 m and 11.10 m between the liquid hydrogen target and the neutron detector and at 3.83 m and 8.40 m in gaseous hydrogen, are displayed in Figs. 3 and 4, respectively. In both cases, the expected step in the TOF-distribution from the Coulomb de-excitation transition $3 \rightarrow 2$ ($T_{\pi p}$ = 209 eV) is clearly visible. From the resulting TOF-spectra, we have obtained the kinetic energy distribution $f(T_{\pi p})$ using three different methods.

In method A, based on the TOF-distribution model [cf. Fig. 1(b)], the three spectra measured in liquid hydrogen were fitted simultaneously by TOF-distributions generated by a detailed GEANT Monte Carlo programme [17] which accounted for the stopping distribution in the target, geometric effects (intrinsic time resolution) and neutron scattering. Similarly, the two spectra measured in gaseous hydrogen were fitted to their respective Monte Carlo distributions. The fit to the data taken with liquid hydrogen was restricted to a region from -15 to $+1$ ns at 3.82 m, from -25 to $+2$ ns at 8.39 m and from -30 to $+2$ ns at 11.10 m to minimize the contributions from scattered neutrons. For the data taken with gaseous hydrogen, the corresponding fit regions were from -15 to $+2$ ns at 3.83 m and from -25 to $+2$ ns at 8.40 m. The free parameters were: (i) four yields corresponding to the Coulomb

de-excitation transitions with principal quantum numbers $6 \to 5$, $5 \to 4$, $4 \to 3$, and $3 \to 2$; (ii) two yields for the Coulomb de-excitation transitions $6 \to 4$ and $5 \to 3$ with $\Delta n = 2$; (iii) the energy parameter T_1 [cf. Fig. 1(a)]; (iv) a distance independent Gaussian time-jitter corresponding to electronic contributions to the time resolution of the detector system; (v) two (H_2 gas) or three (LH_2) normalization factors for the ordinates, and (vi) two (H_2 gas) or three (LH_2) shifts to match the time scales of the experimental histograms; (vii) a yield for all Coulomb de-excitation transitions with $n > 6$; (viii) in the case of liquid hydrogen, we have introduced an upper energy bound for the above transitions, whereas in the case of gaseous hydrogen this corresponds to the mean energy of these transitions.

The difference between the predicted and the observed transition energies $T_{nn'}$ reported in Ref. [5] can be accounted for and made to vanish in our present analysis if we include the $\Delta n = 2$ Coulomb de-excitation transitions. Then, the resultant energies $T_{nn'}$ [cf. Eq. (1)] for $n \leq 6$ perfectly match the theoretical values derived for Coulomb de-excitation and do not have to be taken as free parameters. These fits gave a χ^2/DOF of 0.96 with 740 degrees of freedom (DOF) for the measurements in liquid hydrogen and a χ^2/DOF of 0.96 with 430 DOF for the measurements in hydrogen gas; these correspond to confidence levels of 77.7 % and 72.2 %, respectively. The values for the relative yields $A_{nn'}$ of the transitions are listed in Table 1. For the low energy component of $f(T_{\pi p})$, we found $T_1 = (1.0 \pm 0.1)$ eV for liquid hydrogen and $T_1 = (1.6 \pm 0.2)$ eV for gaseous hydrogen. The upper energy bound for the sum of all Coulomb de-excitation transitions with $n > 6$ is $T_{n>6} = (8 \pm 1)$ eV for liquid hydrogen and in the case of gaseous hydrogen, equivalent to a mean energy, $T_{n>6} = (7 \pm 2)$ eV.

For comparison, fits were made not including the Coulomb de-excitation components with $\Delta n = 2$ (see Table 1). These fits gave in liquid hydrogen a χ^2/DOF of 1.06 with 742 DOF which corresponds to a confidence level of 13.1 % and in gaseous hydrogen a χ^2/DOF of 0.96 with 432 DOF (c.l. = 72.3 %). The differences in the χ^2/DOF between the two sets of fits are not very significant; however, there is a strong hint for components with $\Delta n = 2$ from two other model independent methods (B, C) used in the analysis to extract the kinetic energy distribution $f(T_{\pi p})$ from the data.

In method B, no assumptions about the positions of the peaks were made. Here, the data measured in liquid and gaseous hydrogen were fitted using a kinetic en-

ergy distribution consisting of 16 energy bins (from T_{i-1} to T_i) corresponding to 16 equidistant time bins (from τ_{i-1} to τ_i). The kinetic energy distribution $f(T_{\pi p})$ was assumed to be constant within each bin. The relationship between the time τ_i and the energy T_i is given as in Eq. (2) with $T_i\,[\mathrm{eV}] = i^2$ $(i = 1, \ldots, 16)$. The fit was restricted to the same regions in the TOF-spectra as described above. The resulting kinetic energy distributions are shown in Fig. 5. The yields A_i correspond to the height of the respective bins.

In both kinetic energy distributions, a sharp decrease after the transition $4 \rightarrow 3$ and indications for discrete peaks due to Coulomb de-excitation can be seen. Moreover, in the kinetic energy distribution for liquid hydrogen, a small peak in the region between 100 eV and 121 eV is visible which could be assigned to the Coulomb de-excitation transition $5 \rightarrow 3$ corresponding to an energy of 107 eV. In the distribution for gaseous hydrogen, the error bars are larger due to the lower statistics.

Method C is based on the direct reconstruction of the kinetic energy distribution from the deconvoluted TOF-spectra. Here, the TOF-spectra are deconvoluted with Monte Carlo generated TOF-distributions; neutron scattering, the intrinsic time resolution as well as a distance independent Gaussian time-jitter corresponding to electronic contributions to the time resolution were taken into account. From these monotonously decreasing, deconvoluted TOF-distributions $F(\tau)$, we have calculated the cumulative energy distributions $W(T_{\pi p})$ which are given by

$$W(T_{\pi p}) = 2 \int_0^{\xi\sqrt{T_{\pi p}}} F(\tau) d\tau \; - 2\,\xi\sqrt{T_{\pi p}}\, F(\xi\sqrt{T_{\pi p}}) \tag{3}$$

with $\xi = \frac{l}{v_0^2}\sqrt{\frac{2}{M_{\pi p}}}$. For the calculation of $W(T_{\pi p})$, only the fast side of the neutron TOF-spectra was used to minimize contributions from scattered neutrons. Finally, the kinetic energy distributions $f(T_{\pi p})$ can be calculated as follows[2]:

$$f(T_{\pi p}) = \frac{d}{dT_{\pi p}} W(T_{\pi p}). \tag{4}$$

The final results shown in Fig. 6 were obtained by averaging the kinetic energy distributions for the three different distances in liquid and the two distances in gaseous hydrogen. The shapes of these distributions are consistent with those of Fig. 5.

[2]The kinetic energy distribution could be calculated directly as follows: $f(T_{\pi p}) = -\xi^2 \frac{d}{d\tau} F(\tau)$; however, for technical reasons, we have calculated $W(T_{\pi p})$ first.

In conclusion, we have confirmed the existence of strong 'high-energy' components ($T_{\pi p} \gg 1\,\mathrm{eV}$) in the kinetic energy distribution $f(T_{\pi p})$ of $\pi^- p$-atoms in both liquid and gaseous hydrogen at the instant of the CEX-reaction. The results obtained from three different methods of reconstruction of the energy distributions are self-consistent. These 'high-energy' components contain about half of the $\pi^- p$-atoms (see Table 1), and about four percent have kinetic energies as high as $\simeq 200\,\mathrm{eV}$. The shapes of the energy distributions strongly support the Coulomb de-excitation like origin of the 'high-energy' components and further give evidence for $\Delta n = 2$ Coulomb transitions. The inclusion of the $\Delta n = 2$ Coulomb de-excitation components in the present analysis make the previously claimed energy shifts in $T_{nn'}$ [5] vanish. Our results favour the recent calculations of the Coulomb de-excitation process [18, 19], which predict relatively high rates and resolve a long standing discrepancy between past calculations [11, 14, 20–22].

We thank Z. Hochman, L. Knecht and H. Obermeier for their very competent technical assistance. The support from the Hallendienst and many other PSI staff members is gratefully acknowledged. This experiment was supported by the Schweizerischer Nationalfonds zur Förderung der wissenschaftlichen Forschung.

References

[1] J. B. Czirr, Phys. Rev. 130 (1963) 341.

[2] J. F. Crawford et al., Phys. Rev. Lett. 56 (1986) 1043.

[3] J. F. Crawford et al., Phys. Lett. B 213 (1988) 391.

[4] J. F. Crawford et al., Phys. Rev. D 43 (1991) 46.

[5] A. Badertscher et al., Phys. Lett. B 392 (1997) 278.

[6] E. C. Aschenauer et al., Phys. Rev. A 51 (1995) 1965.

[7] D. Chatellard et al., Phys. Rev. Lett. 74 (1995) 4157.

[8] D. Chatellard et al., Nucl. Phys. A 625 (1997) 855.

[9] D. Sigg et al., Phys. Rev. Lett. 75 (1995) 3245.

[10] D. Sigg et al., Nucl. Phys. A 609 (1996) 269.

[11] L. Bracci and G. Fiorentini, Nuovo Cimento 43A (1978) 9.

[12] P. Froelich and J. Wallenius, Phys. Rev. Lett. 75 (1995) 2108.

[13] J. Wallenius and P. Froelich, Proceedings of EXAT98 (to be published in Hyperfine Interactions, 1999).

[14] L. I. Men'shikov, Muon Catalyzed Fusion 2 (1988) 173.

[15] R. Frosch, PSI Internal report TM-37-21 (1985), unpublished.

[16] A. Bay et al., Nucl. Instr. Meth. in Phys. Res. A 271 (1988) 497.

[17] GEANT - Detector Description and Simulation Tool, CERN Program Library.

[18] A.V. Kravtsov, Proceedings of EXAT98 (to be published in Hyperfine Interactions, 1999).

[19] E.A. Solov'ev, Proceedings of EXAT98 (to be published in Hyperfine Interactions, 1999).

[20] W. Czaplinski et al., Muon Catalyzed Fusion 5/6 (1990) 59.

[21] W. Czaplinski et al., Phys. Rev. A 50 (1994) 525.

[22] L. I. Ponomarev and E. A. Solov'ev, JETP Lett. 64 (1996) 135.

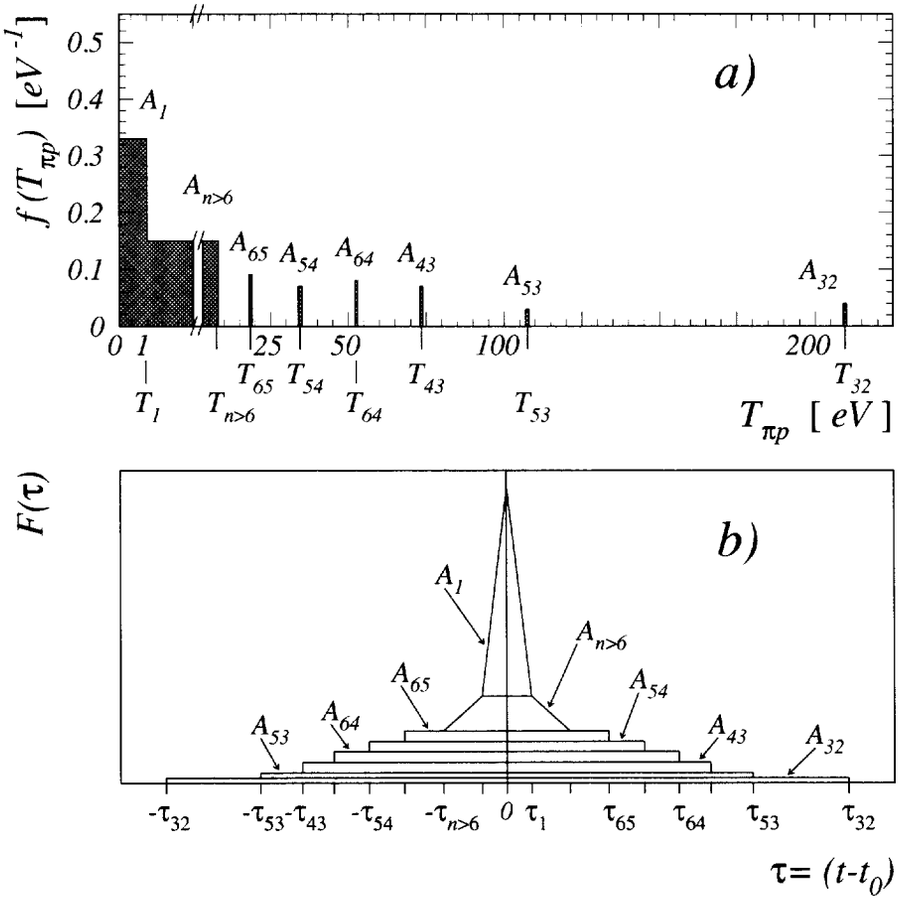

Figure 1: (a) Idealized distribution function $f(T_{\pi p})$ of the kinetic energy $T_{\pi p}$ of pionic hydrogen atoms at the instant of nuclear capture. Here, T_1 and the widths of the six δ-like peaks at $T_{nn'}$ are drawn to be 1 eV wide. The integrals of these peaks correspond to the relative yields A_1 and $A_{nn'}$, respectively. (b) Neutron TOF-distribution $F(\tau)$ corresponding to the kinetic energy distribution of Fig. 1(a).

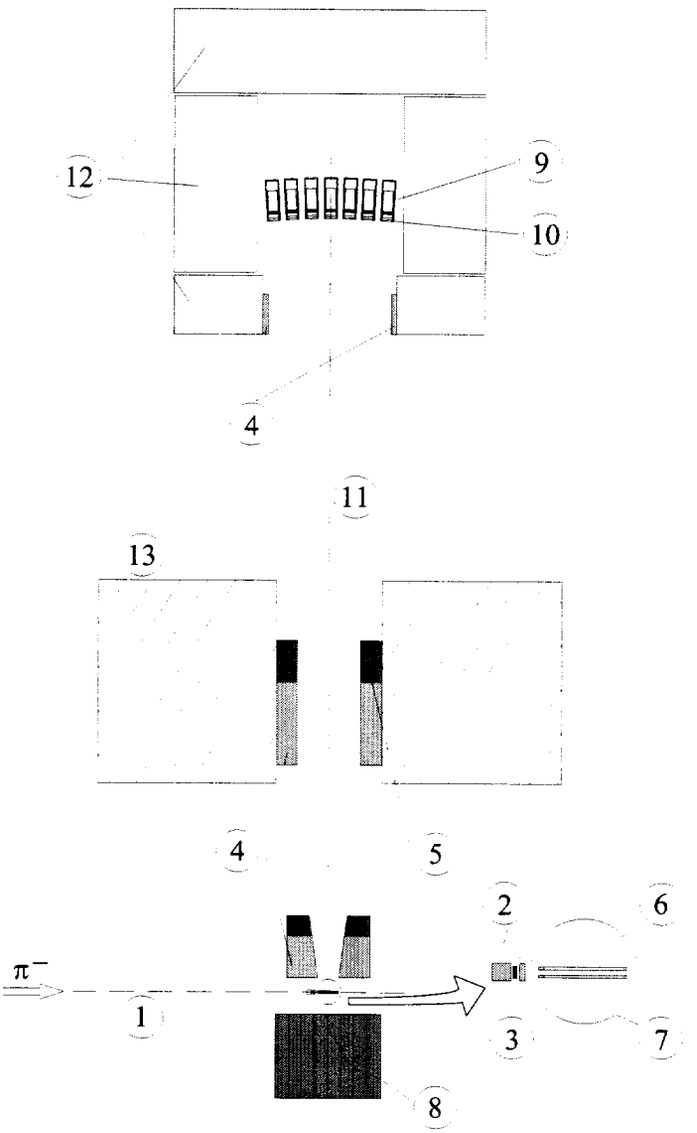

Figure 2: Experimental setup. 1) central pion trajectory; 2) carbon degrader; 3) scintillator S1; 4) CH_2-collimator; 5) lead collimator; 6) hydrogen target; 7) vacuum vessel of the LH_2-target; 8) NaI-crystals (8×8 matrix) for the detection of photons from the π^0-decay; 9) photomultiplier tubes; 10) neutron detection scintillators; 11) central neutron trajectory; 12) CH_2 and lead shielding; 13) concrete shielding.

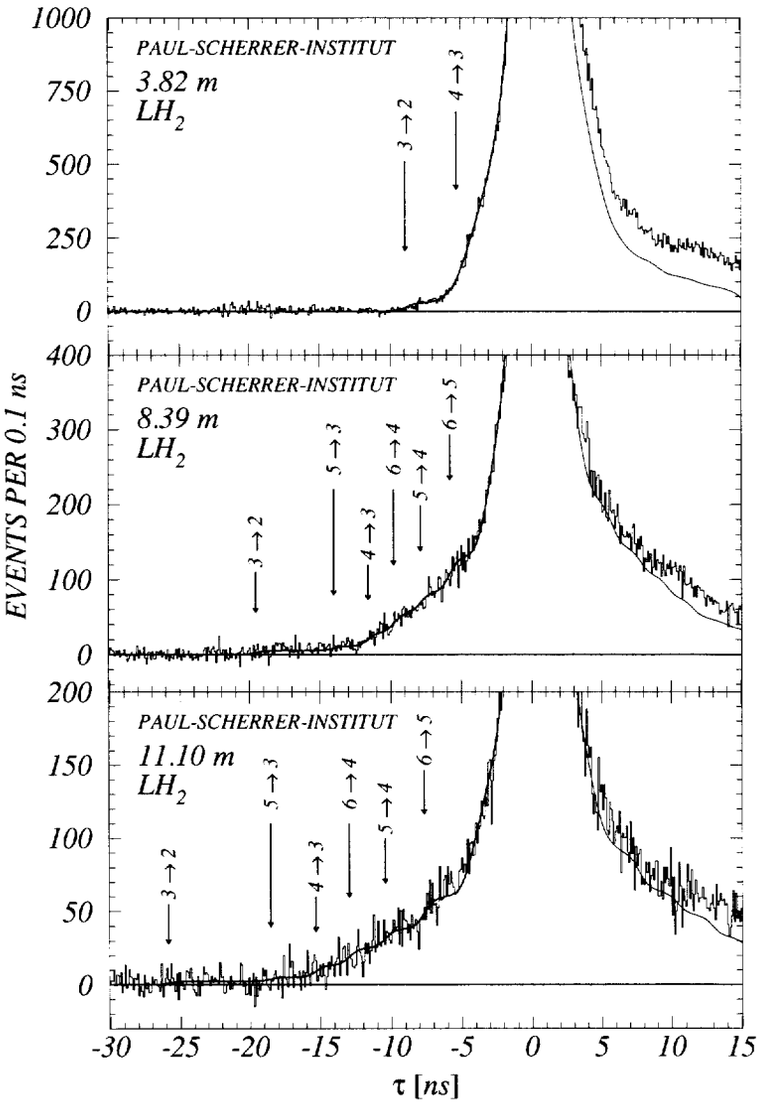

Figure 3: Histograms: measured TOF-spectra from the charge exchange reaction $\pi^- p \rightarrow \pi^0 + n$ in liquid hydrogen (LH_2), after background subtraction, for flight-paths 3.82 m, 8.39 m and 11.10 m. The time is measured from the centre of the neutron peak corresponding to the reaction at rest. Curves: fits to the data including Coulomb de-excitation process. The numbers $n \rightarrow n'$ indicate the fitted positions of the steps in the TOF-distribution of neutrons which are emitted after the corresponding Coulomb de-excitation transition.

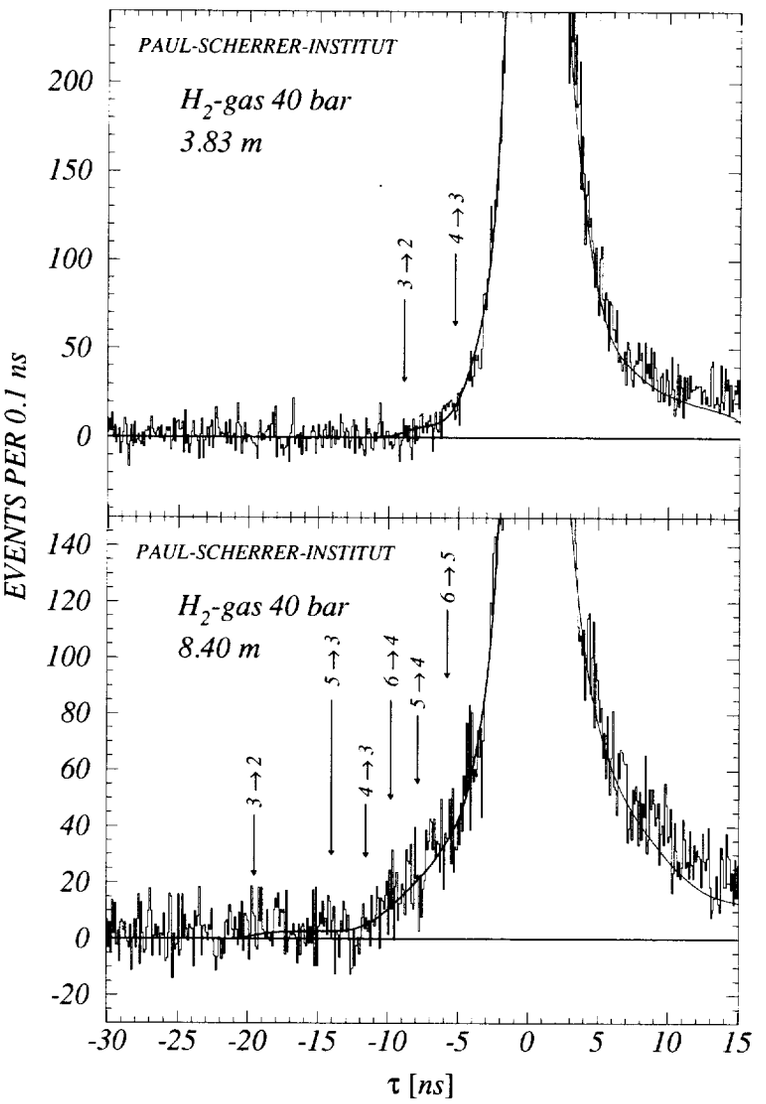

Figure 4: Same as Fig. 3; for the measurements in 40 bar hydrogen gas the flight-paths are 3.83 m and 8.40 m.

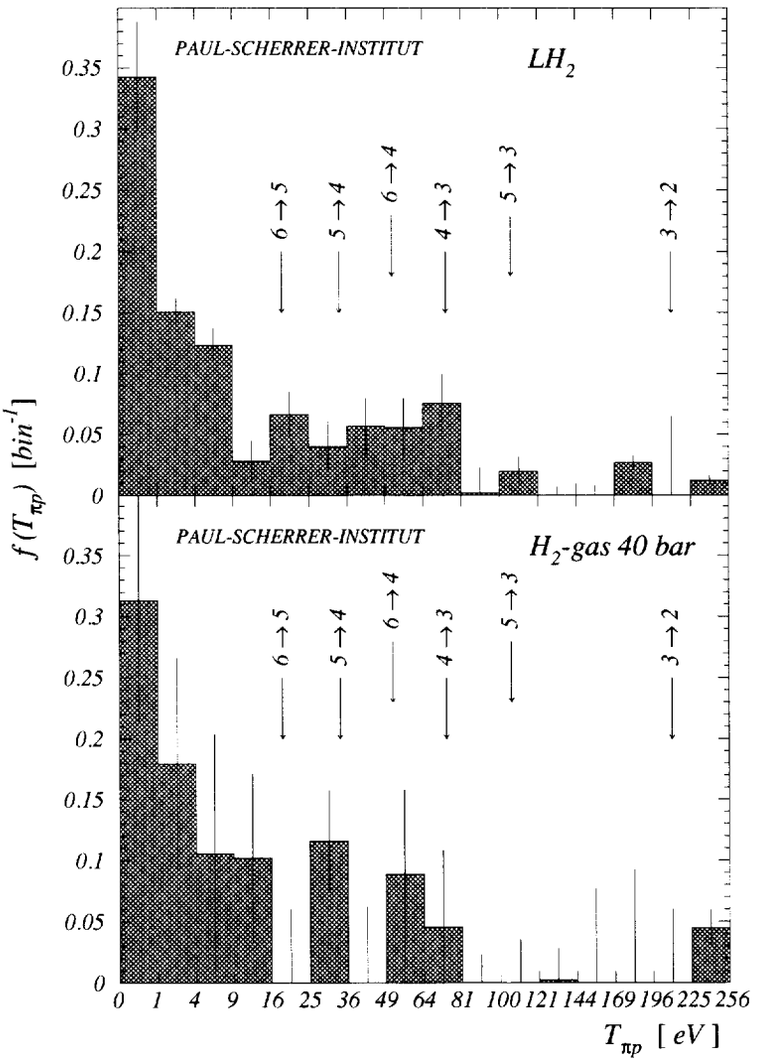

Figure 5: Model independent kinetic energy distribution $f(T_{\pi p})$ for liquid and gaseous hydrogen obtained by fitting 16 kinetic energy bins to the measured TOF-spectra. The numbers $n \rightarrow n'$ indicate the positions of the theoretical values of the kinetic energy for the $\pi^- p$-atoms derived for the Coulomb de-excitation process. The errors of the yields are indicated by vertical lines.

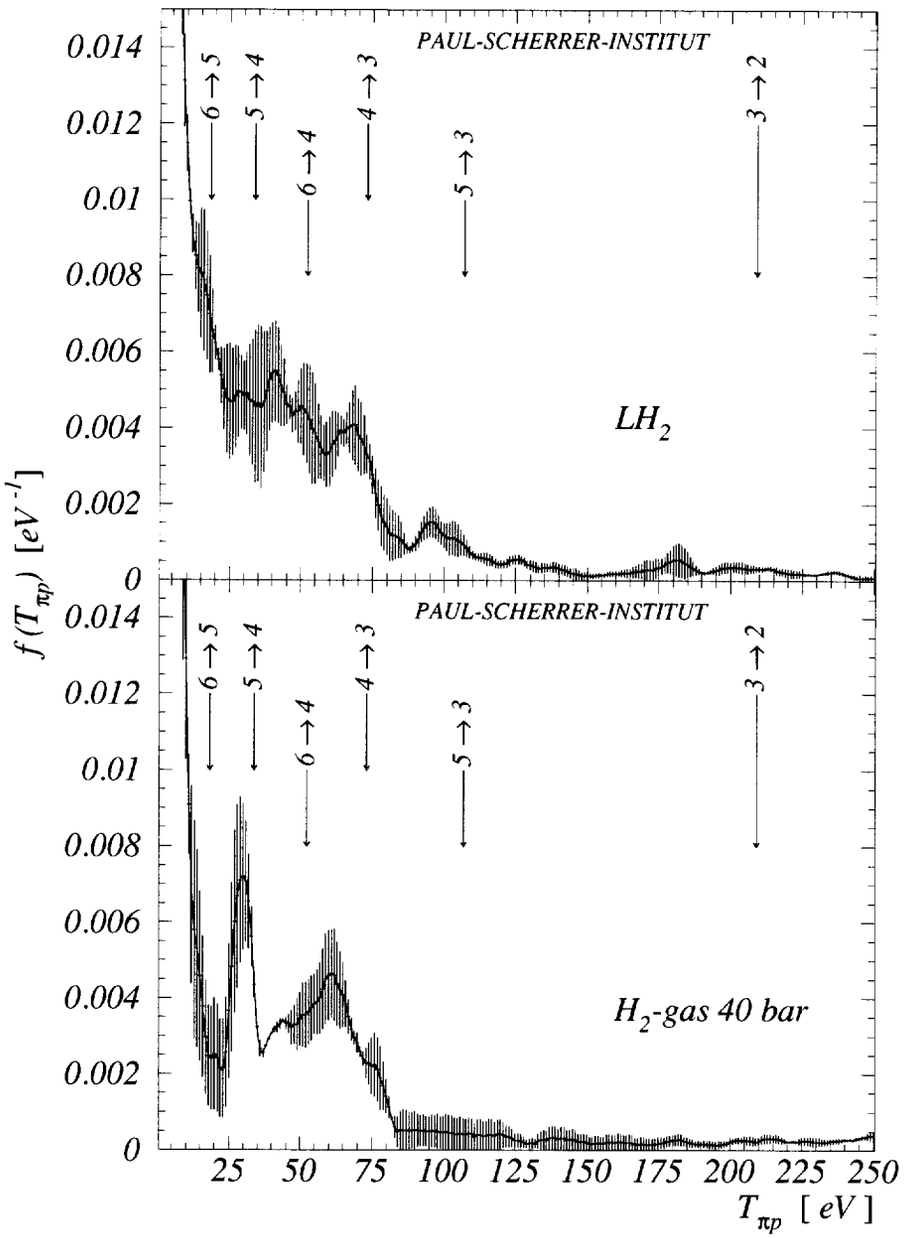

Figure 6: Kinetic energy distribution $f(T_{\pi p})$ for liquid and gaseous hydrogen calculated from the deconvoluted TOF-spectra. The numbers $n \rightarrow n'$ indicate the positions of the theoretical values of the kinetic energy for the $\pi^- p$-atoms derived for the Coulomb de-excitation process.

transition	energy	$A_{nn'}$ [%]			
$n \to n'$	$T_{n,n'}$ [eV]	LH_2	H_2 gas	LH_2	H_2 gas
$n > 6$	< 18.4	27 ± 2	19 ± 5	26 ± 2	21 ± 5
$6 \to 5$	18.4	9 ± 1	9 ± 3	7 ± 1	6 ± 3
$5 \to 4$	33.9	7 ± 1	7 ± 4	12 ± 1	14 ± 3
$4 \to 3$	73.2	7 ± 1	5 ± 3	14 ± 1	10 ± 2
$3 \to 2$	209.1	3 ± 1	5 ± 1	4 ± 1	4 ± 1
$6 \to 4$	52.3	8 ± 1	9 ± 4	not fitted	not fitted
$5 \to 3$	107.1	3 ± 1	0^{+2}_{-0}	not fitted	not fitted
χ^2/DOF		0.96	0.96	1.06	0.96
c. l. [%]		77.7	72.2	13.1	72.3
T_1		1.0±0.1	1.6±0.2	1.0±0.1	1.5±0.3
$T_{n>6}$ [eV]		7.6±0.3	6.7±2.2	7.9±0.4	6.8±2.3

Table 1: Fitted yields $A_{nn'}$ of Coulomb de-excitation peaks in the kinetic energy distribution $f(T_{\pi p})$ for the transitions $n \to n'$ in liquid and gaseous hydrogen. Fit results including $\Delta n = 2$ (left) and $\Delta n = 1$ only (right).